Electronic Supplementary Material (ESI) for Journal of Materials Chemistry C.
This journal is © The Royal Society of Chemistry 2019

Supporting Information

In-Situ Monitoring of the Charge Carrier Dynamics of $CH_3NH_3PbI_3$ Perovskite Crystallization Process

Efthymis Serpetzoglou[1,3,], Ioannis Konidakis[1], Temur Maksudov[2,4], Apostolos Panagiotopoulos[2,4], Emmanuel Kymakis[2], Emmanuel Stratakis[1,4,*]*

[1]Institute of Electronic Structure and Laser (IESL), Foundation for Research and Technology-Hellas (FORTH), 71110, Heraklion, Crete, Greece

[2]Center of Materials Technology and Photonics, Electrical Engineering Department, Technological Educational Institute (TEI) of Crete, 71004, Heraklion, Crete, Greece

[3]Department of Physics, University of Crete, Herakleio, Greece

[4]Department of Materials Science and Technology, University of Crete, Greece, 71003, Heraklion, Crete, Greece

Corresponding Authors

*+30 2810-391274. E-mail: stratak@iesl.forth.gr

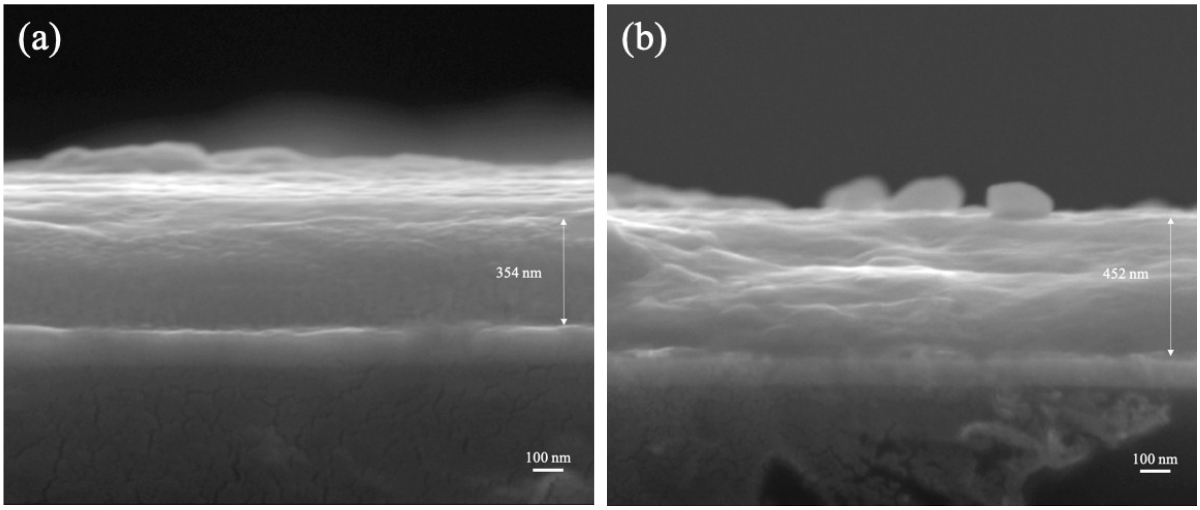

Figure S1: Cross-section SEM images for IS samples at 100 ºC for PEDOT:PSS/$CH_3NH_3PbI_3$ **(a)** and PTAA/$CH_3NH_3PbI_3$ **(b)** configurations.

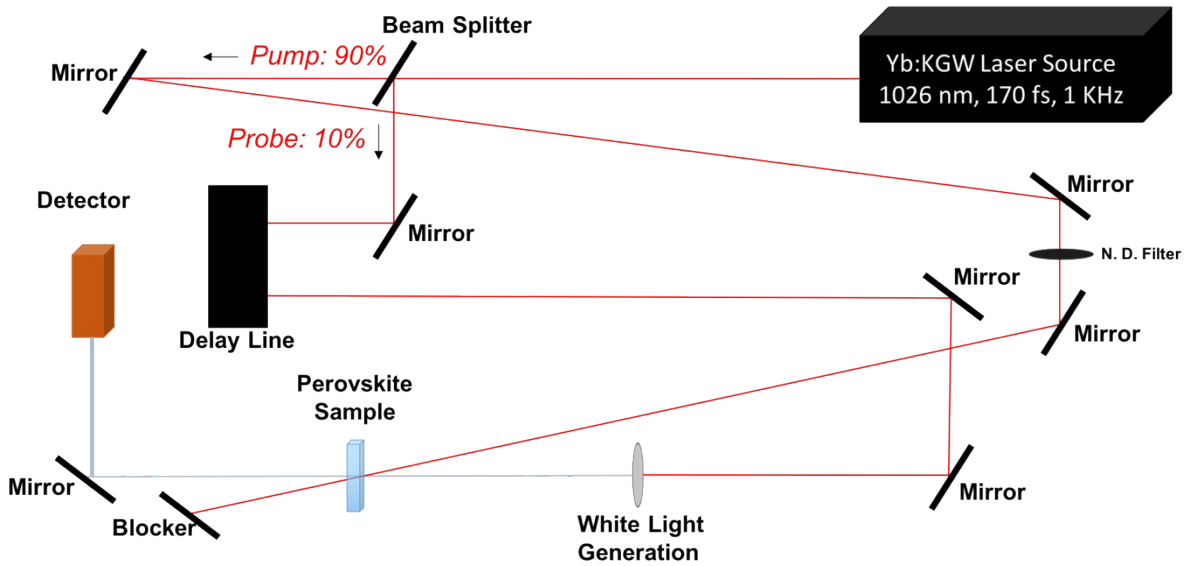

Figure S2. Schematic representation of Newport transient absorption spectrometer (TAS-1).

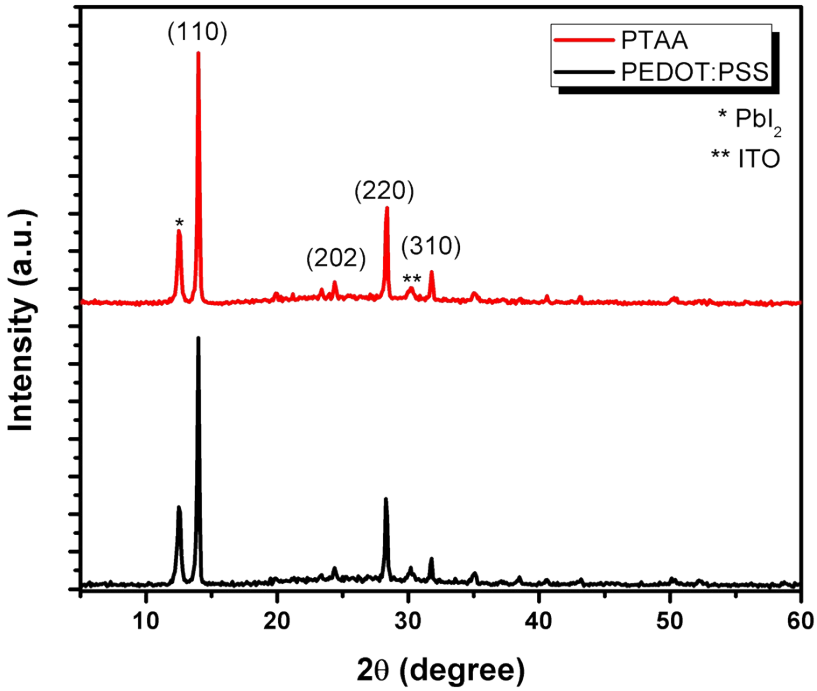

Figure S3: XRD patterns of the thermal annealing PEDOT:PSS/$CH_3NH_3PbI_3$ and PTAA/$CH_3NH_3PbI_3$ architectures. (copyright Serpetzoglou et al. *ACS Appl. Mater. Interfaces*, 2017, **9**, 43910).

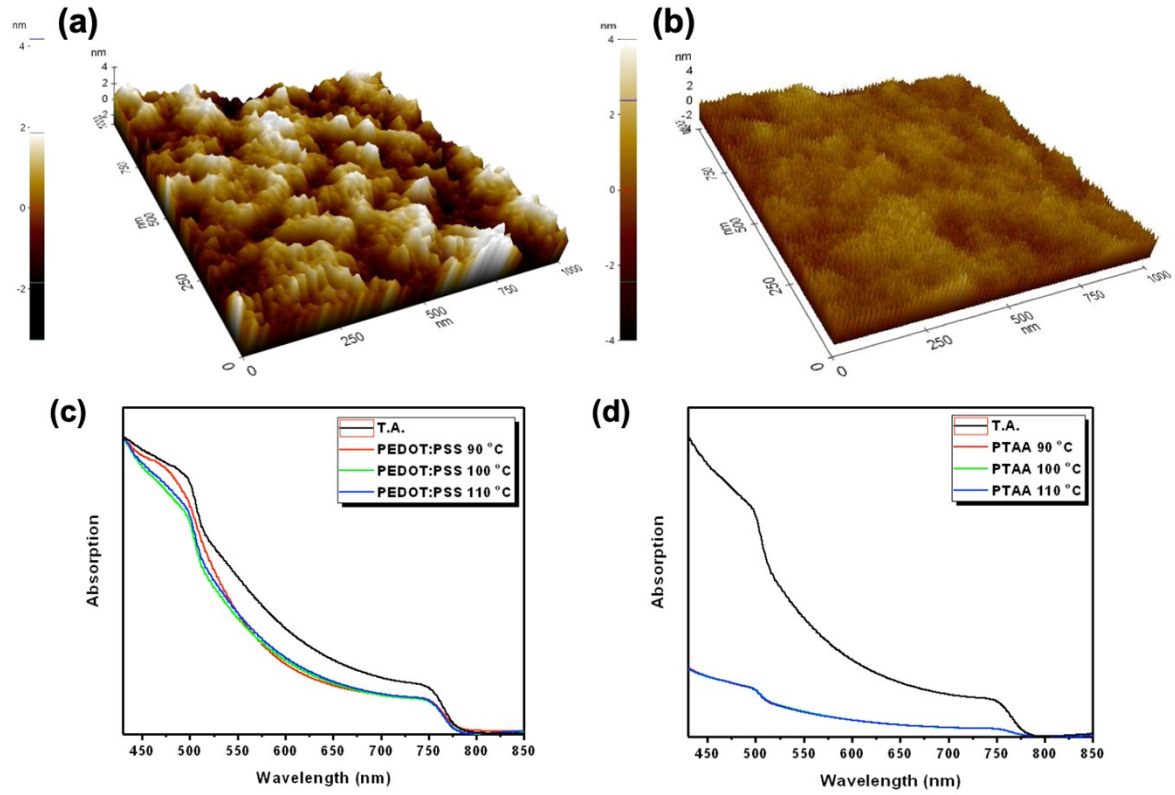

Figure S4: AFM measurements of the PEDOT:PSS (a) and PTAA (b) polymers. Absorption spectra for PEDOT:PSS/$CH_3NH_3PbI_3$ (c) and PTAA/$CH_3NH_3PbI_3$ (d) configurations for TA and IS samples.

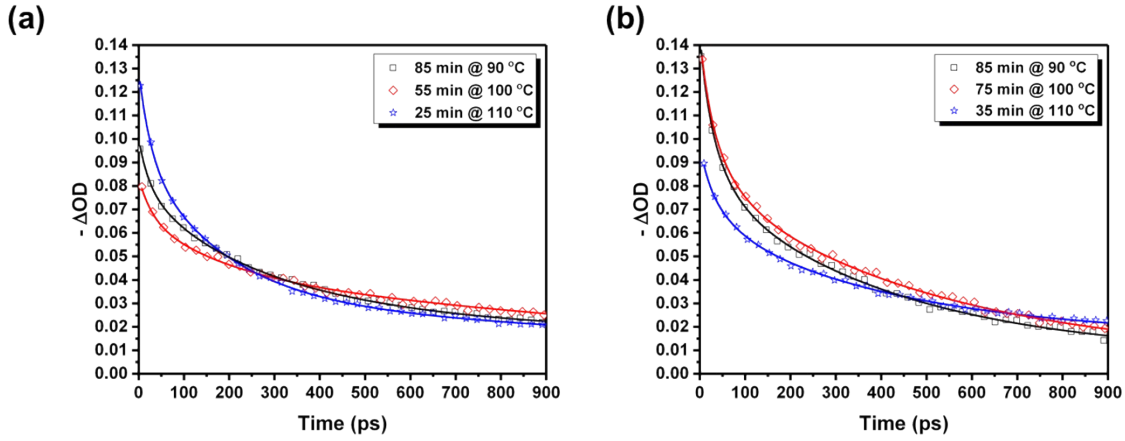

Figure S5: Transient band edge bleach kinetics (symbols) and the corresponding polynomial fittings PEDOT:PSS/$CH_3NH_3PbI_3$ (a) and for PTAA/$CH_3NH_3PbI_3$ (b) at the optimum crystallization period, photoexcited at 1026 nm with a pump fluence of 1.5 mJ cm^{-2}.

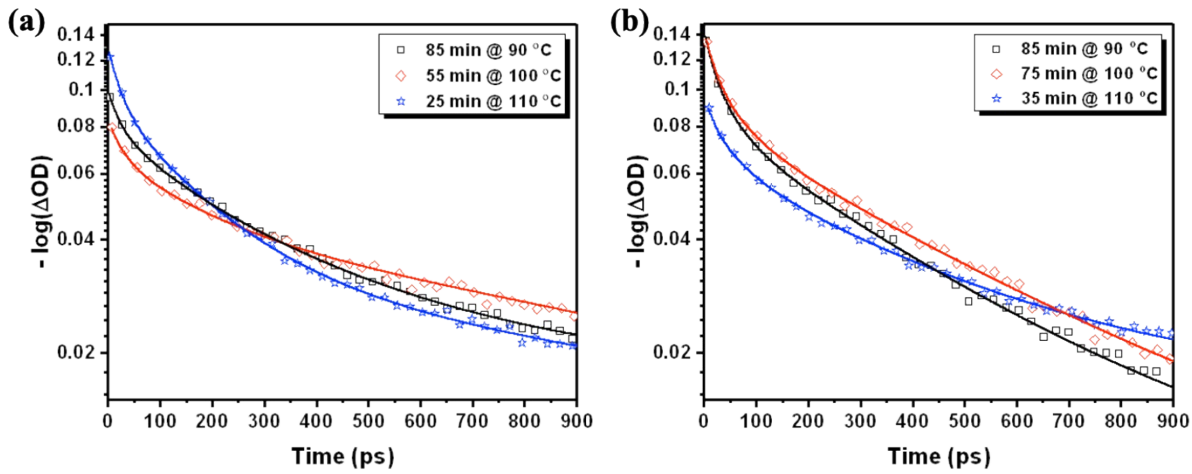

Figure S6: Logarithmic transient band edge bleach kinetics (symbols) and the corresponding polynomial fittings PEDOT:PSS/$CH_3NH_3PbI_3$ (a) and for PTAA/$CH_3NH_3PbI_3$ (b) at the optimum crystallization period, photoexcited at 1026 nm with a pump fluence of 1.5 mJ cm^{-2}.

Table S1: $CH_3NH_3PbI_3/PbI_2$ peak ratios from XRD patterns for all IS studied samples.

Architecture	Annealing Temperature	$CH_3NH_3PbI_3/PbI_2$ Peak Ratio
PEDOT:PSS/ $CH_3NH_3PbI_3$	90 °C	2.83
PEDOT:PSS/ $CH_3NH_3PbI_3$	100 °C	2.21
PEDOT:PSS/ $CH_3NH_3PbI_3$	110 °C	2.20
PTAA/ $CH_3NH_3PbI_3$	90 °C	1.37
PTAA/ $CH_3NH_3PbI_3$	100 °C	1.58
PTAA/ $CH_3NH_3PbI_3$	110 °C	1.63

TAS Fitting Analysis

We choose the appropriate equation and fitting model (ExpDec3) because there are three different phenomena that take place in the solar cell device when it's irradiated by light, the charge carrier trapping (τ_1), the hole injection (τ_2) and the exciton recombination (τ_3). Before we fit our data, we narrow the range of τ_1 and τ_2 and y_0. Specifically, we narrow the time ranges for τ_1, τ_2, from 10 ps up to 30 ps and from 30 ps up to 200 ps, respectively, for both configurations in order to obtain fast and efficient hole injection from the perovskite layer to hole transport layer. Moreover, we narrow also the constant, y_0, of our equation between 0 and the lowest value of ΔOD, because in the time range of our setup is impossible not to have excited electrons in the conduction band of the perovskite layer.

Additionally, in **Tables S2,3** we present the further analysis at optimum annealing period at 90 °C for both configurations for tri-exponential fitting model that we use. We have to mention that the same trend observed also for 100 °C and 110 °C for both architectures. Especially, in **Tables S2,3 (a)** we show the optimum fitting without any fixed term (fitting software internal

algorithm provides best fit, only from a mathematical point of view). **Tables S2,3 (b)** present the time components in which the y_0 and τ_1 are fixed in the values from the optimum fitting. We obtain that the deviation of τ_2 and τ_3 is within the error that we have already presented in the revised manuscript. Moreover, **Tables S2,3 (c)** show the corresponding fitting when only τ_2 is fixed in the optimum value. With this procedure, we take unrealistic τ_1 and τ_3 for the perovskite solar cell. Finally, in **Tables S2,3 (d, f)** we present the time components when the τ_3 is fixed with lower and higher compared with the τ_3 value extracting from the optimum value, respectively. In both cases the τ_2 value is too slow to present the hole injection from the perovskite to the hole transport layer.

(a) Model	ExpDec3
Equation	$y = A_1*\exp(-x/\tau_1) + A_2*\exp(-x/\tau_2) + A_3*\exp(-x/\tau_3) + y_0$
Plot	deltaOD
y_0	0.01753 ± 6.10E-4
τ_1	21.85 ± 1.89
τ_2	105.16 ± 7.45
τ_3	3.2E7 ± 12.60
Adj. R-Square	0.9983

(b) Model	ExpDec3
Equation	$y = A_1*\exp(-x/\tau_1) + A_2*\exp(-x/\tau_2) + A_3*\exp(-x/\tau_3) + y_0$
Plot	deltaOD
y_0	0.018 ± 0
τ_1	22 ± 0
τ_2	97.83 ± 6.45
τ_3	3.1E7 ± 4.89
Adj. R-Square	0.9983

(c) Model	ExpDec3
Equation	$y = A_1*\exp(-x/\tau_1) + A_2*\exp(-x/\tau_2) + A_3*\exp(-x/\tau_3) + y_0$
Plot	deltaOD
y_0	0.01298 ± 0.00637
τ_1	577.19 ± 7.1E6
τ_2	22 ± 0
τ_3	577.22 ± 6.36E6
Adj. R-Square	0.9958

(d) Model	ExpDec3
Equation	$y = A_1*\exp(-x/\tau_1) + A_2*\exp(-x/\tau_2) + A_3*\exp(-x/\tau_3) + y_0$
Plot	deltaOD
y_0	0.01303 ± 0.00379
τ_1	26.3 ± 1.3
τ_2	980.1 ± 422.1
τ_3	1.4E7 ± 0
Adj. R-Square	0.9982

(e) Model	ExpDec3
Equation	$y = A_1*\exp(-x/\tau_1) + A_2*\exp(-x/\tau_2) + A_3*\exp(-x/\tau_3) + y_0$
Plot	deltaOD
y_0	0.001835 ± 0.0013
τ_1	21.85 ± 1.96
τ_2	105.3 ± 7.94
τ_3	3.2E7 ± 0
Adj. R-Square	0.9983

(f) Model	ExpDec3
Equation	$y = A_1*\exp(-x/\tau_1) + A_2*\exp(-x/\tau_2) + A_3*\exp(-x/\tau_3) + y_0$
Plot	deltaOD
y_0	0.01507 ± 4.4E-4
τ_1	24.51 ± 1.54
τ_2	204.34 ± 13.59
τ_3	8.4E7 ± 0
Adj. R-Square	0.9983

Table S2: Fitting analysis at optimum annealing period at 90 ^{o}C for PEDOT:PSS/$CH_3NH_3PbI_3$ configuration, **(a)** the optimum fitting, **(b)** y_0 and τ_1 are fixed, **(c)** τ_2 is fixed, and **(d-f)** τ_3 is fixed.

(a) Model	ExpDec3
Equation	$y = A_1*\exp(-x/\tau_1) + A_2*\exp(-x/\tau_2) + A_3*\exp(-x/\tau_3) + y_0$
Plot	deltaOD
y_0	0.00758 ± 5.48E-4
τ_1	17.02 ± 1.95
τ_2	48.27 ± 7.85
τ_3	418.91 ± 12.60
Adj. R-Square	0.9978

(b) Model	ExpDec3
Equation	$y = A_1*\exp(-x/\tau_1) + A_2*\exp(-x/\tau_2) + A_3*\exp(-x/\tau_3) + y_0$
Plot	deltaOD
y_0	0.01 ± 0
τ_1	17 ± 0
τ_2	40.09 ± 2.79
τ_3	371.2 ± 2.3
Adj. R-Square	0.9977

(c) Model	ExpDec3
Equation	$y = A_1*\exp(-x/\tau_1) + A_2*\exp(-x/\tau_2) + A_3*\exp(-x/\tau_3) + y_0$
Plot	deltaOD
y_0	0.0055 ± 0.0029
τ_1	467.2 ± 8.1E5
τ_2	48 ± 0
τ_3	467.2 ± 7.4E5
Adj. R-Square	0.9971

(d) Model	ExpDec3
Equation	$y = A_1*\exp(-x/\tau_1) + A_2*\exp(-x/\tau_2) + A_3*\exp(-x/\tau_3) + y_0$
Plot	deltaOD
y_0	0.0053 ± 0.0025
τ_1	33.03 ± 1.2
τ_2	575.9 ± 132.9
τ_3	250 ± 0
Adj. R-Square	0.9977

(e) Model	ExpDec3
Equation	$y = A_1*\exp(-x/\tau_1) + A_2*\exp(-x/\tau_2) + A_3*\exp(-x/\tau_3) + y_0$
Plot	deltaOD
y_0	0.00758 ± 1.3E-4
τ_1	17.02 ± 4.81
τ_2	48.29 ± 5.10
τ_3	419 ± 0
Adj. R-Square	0.9978

(f) Model	ExpDec3
Equation	$y = A_1*\exp(-x/\tau_1) + A_2*\exp(-x/\tau_2) + A_3*\exp(-x/\tau_3) + y_0$
Plot	deltaOD
y_0	0.0046 ± 0.0011
τ_1	32.61 ± 1.35
τ_2	239.96 ± 40.24
τ_3	600 ± 0
Adj. R-Square	0.9977

Table S3: Fitting analysis at optimum annealing period at 90 ^{o}C for PTAA/$CH_3NH_3PbI_3$ configuration, **(a)** the optimum fitting, **(b)** y_0 and τ_1 are fixed, **(c)** τ_2 is fixed, and **(d-f)** τ_3 is fixed.

In order to eliminate any doubts about the fitting uncertainties in **Table S4,5** we present the lower and upper limit for each time component for both configuration. In case of

PEDOT:PSS/$CH_3NH_3PbI_3$ architecture the errors for the τ_1, τ_2 and τ_3 are 2 ps, 8 ps and 0.5E7 ps, respectively. While in case of PTAA/$CH_3NH_3PbI_3$ configuration the errors for the τ_1, τ_2 and τ_3 are 2 ps, 8 ps and 13 ps, respectively. Within these limits we obtain values for time components that are reasonable for the operation of the perovskite solar cell. Firstly, we initiate an upper and a lower limit of τ_1 at values that are physically explainable. The lower and upper limit of τ_1 take values for τ_2 and τ_3. If they are not realistic, we further reduce the upper and lower limits of τ_1, until we reach the value range of τ_1 that gives realistic results for τ_2, τ_3. So, the τ_1 value gives me the error for τ_2 and τ_3 time components. In this way, we have an empirical adaptation that has a physical explanation and is actually shifted.

	Lower Limit	Upper Limit
y_0	Fixed at 0.01753	
τ_1	21 ps	24 ps
τ_2	97 ps	113 ps
τ_3	2.7E7 ps	3.5E7 ps

Table S4: Lower and Upper Limits for time components for PEDOT:PSS/$CH_3NH_3PbI_3$ architecture.

	Lower Limit	Upper Limit
y_0	Fixed at 0.0075	
τ_1	15 ps	19 ps
τ_2	40 ps	56 ps
τ_3	407 ps	431 ps

Table S5: Lower and Upper Limits for time components for PTAA/$CH_3NH_3PbI_3$ architecture.